Published in Journal of Electron Spectroscopy and Related Phenomena 137-140: 687-690, 2004

High-resolution XES and RIXS studies with a von Hamos Bragg crystal spectrometer

J. Hoszowska [a,*], J.-Cl. Dousse [b]

[a] *European Synchrotron Radiation Facility, 6 Jules Horowitz, F-38043 Grenoble, France*
[b] *Department of Physics, University of Fribourg, Ch. du Musée 3, CH-1700 Fribourg, Switzerland*

Available online 20 March 2004

Abstract

The high-resolution von Hamos Bragg crystal spectrometer was constructed for the study of K X-ray emission from low-*Z* elements and L and M X-ray spectra of medium to high *Z* elements. Recently, this instrument was applied to high-resolution XES and RIXS studies using X-ray synchrotron radiation at the ID21 and BM5 beamlines at the ESRF. An outline of the spectrometer design and performance characteristics will be given. The studies deal with the energy dependent KL double photoexcitation of argon, the L_3 and M_1 atomic-level widths of elements $54 \leq Z \leq 77$, and the evolution of the K-edge RIXS spectra of manganese oxides.

Keywords: High-resolution X-ray spectrometer; XES; RIXS; Atomic-level widths; Double photoexcitation

1. Introduction

High-resolution X-ray emission spectroscopy represents a powerful tool for the investigation of electronic properties and the study of inner-shell processes. Indeed, it continues to contribute to our understanding of atomic structures and dynamics as well as of electronic states in solids. With the advent of high-brilliance X-ray synchrotron sources there has been a renewed interest in X-ray emission spectroscopy (XES), and also remarkable progress in experimental techniques, especially in resonant XES also known as resonant inelastic X-ray scattering (RIXS) [1]. For the measurement of X-ray emission spectra high-resolution X-ray spectrometers are mandatory. Various X-ray spectrometer geometries depending on the application and energy range of interest can be employed. In comparison to a dedicated experimental setup at a particular synchrotron beamline, the von Hamos Bragg bent crystal spectrometer [2] has the advantage of being relatively compact and hence suitable for transportation while preserving both high energy resolution and collection efficiency over a wide energy range from 0.55 to 16.8 keV. Thanks to the versatility of this X-ray spectrometer, measurements of X-ray emission spectra using an electron gun or a conventional X-ray source, as well as at charged particle and X-ray synchrotron beamlines are feasible. Ample data have been collected with this instrument over the last years in different areas of research in atomic physics and for the metrology of X-ray transitions (see, e.g., [3–6]). Access to X-ray synchrotron radiation facilities providing intense and tunable monochromatic X-ray beams has incited new research projects. Recently, the high-resolution von Hamos Bragg crystal spectrometer was applied to X-ray emission spectroscopy studies using X-ray synchtrotron radiation at the ID21 and BM5 beamlines at the ESRF. The high-resolution measurements concern the energy-dependent double photoexcitation of argon [7], the reexamination of L_3 and M_1 atomic-level widths as well as data for L_3–$M_{4,5}$ and L_3–M_1 X-ray transition energies of thirteen elements ranging from xenon ($Z = 54$) to iridium ($Z = 77$) [8], and the investigation of K-edge RIXS spectra of metallic manganese and several manganese oxides that is being pursued.

2. X-ray spectrometer design and characteristics

A detailed description of the von Hamos Bragg crystal X-ray spectrometer can be found in [2]. In the following an outline of the spectrometer design and performance characteristics will be given.

* Corresponding author. Tel.: +33-476-88-2212; fax: +33-476-88-2325.
E-mail address: hoszowska@esrf.fr (J. Hoszowska).

0368-2048
doi:10.1016/j.elspec.2004.02.005

The principal elements of the instrument are the X-ray source defined by a rectangular slit, a cylindrically bent crystal and a position sensitive detector located on the crystal axis of curvature. For a fixed position of the components, an X-ray location on the detector corresponds geometrically to a particular Bragg angle and hence to a particular X-ray energy. The von Hamos geometry permits at one positioning of the spectrometer components data collection over an energy bandwidth limited primarily by the detector length. This bandwidth varies from 30 to 300 eV. To study a greater energy interval the central Bragg angle is adjusted by translation of the crystal and correspondingly of the detector along their axes. The position of the charged-coupled device (CCD) detector is determined by means of an optical device with a precision of $\pm 3\,\mu$m. With a Bragg angular domain of 24.4–61.1°, an X-ray energy range from 0.547 to 16.8 keV can be covered with six different crystals. The crystal laminae, permanently glued to aluminum blocks machined to a precise concave cylindrical surface, have a nominal radius of 25.4 cm. The target, crystal and detector are all contained in a stainless steel vacuum chamber (180 cm × 62 cm × 24.5 cm) pumped down to about 10^{-7} Torr. The energy resolution is typically 1–3 eV depending on the energy, the slit width and the crystal Darwin width.

X-rays are recorded with a CCD position sensitive detector 27.65 mm long and 6.9 mm high, consisting of 1024 columns and 256 rows with a pixel size of 27 μm × 27 μm and having a depletion depth of 50 μm. The detector is cooled thermoelectrically down to −70 °C. The chip was manufactured at EEV (Chelmsford, Essex, CM1 2QU England). For detection of soft X-rays from below 3 keV the spectrometer will be equipped with a scientific grade back-illuminated CCD (MTE:400B camera from Princeton Instruments, vacuum head with E2V CCD 36-40) without antireflection coating, consisting of 1340 × 400 pixels and having 20 μm × 20 μm resolution. The diffracted X-rays hit the CCD and form a 2D intensity image. Since the intensity in each pixel is proportional to the deposited energy, higher-order reflections as well as background and multiple hit events can thus be rejected by setting appropriate energy windows. The data are taken in a repetitive accumulation mode, with acquisition times per frame ranging from one to hundreds of seconds. Each image corresponding to a separate acquisition is filtered and then all the images are summed. The X-ray spectrum is obtained by projection of the final 2D-image on the dispersion axis.

3. Near K-shell threshold argon KL satellite structures studied by XES

Direct photoionization of inner shell electrons in atoms may be accompanied by multielectronic excitations through intra-atomic electron correlations. The second electron can be either ejected to the continuum (shakeoff) or promoted to an unoccupied level (shakeup). The study of shake processes provides information on electron correlations within the atom and is a signature of the breakdown of the independent electron picture. Multielectronic effects can either be investigated by photoabsorption measurements [9] or by means of observing X-ray emission spectra (see, e.g. [10,11]). In the present study high-resolution measurements of KL-$L_{2,3}$L satellite spectra of gaseous argon were carried out. X-ray beam energies in the range from 3455 to 6540 eV were used to investigate the evolution of the K + L double excitation from threshold to saturation. For illustration the Ar KL–$L_{2,3}$L satellite X-ray spectra for three different excitation energies are presented in Fig. 1. The satellite line shapes and their evolution with the excitation energy were analyzed with the aid of MCDF (multiconfiguration Dirac-Fock) calculations.

The excitation probabilities were deduced from the fitted satellite-to-diagram line yield ratios. The determined experimental probabilities were compared to theoretical predictions based on the model of Thomas [12]. In this model the probability for either exciting or ionizing an electron from a bound core-orbital as a result of inner-shell vacancy production can be calculated from the adiabatic to the sudden regime. Separate 2p and 2s Thomas functions were employed to fit our experimental probabilities. Results are

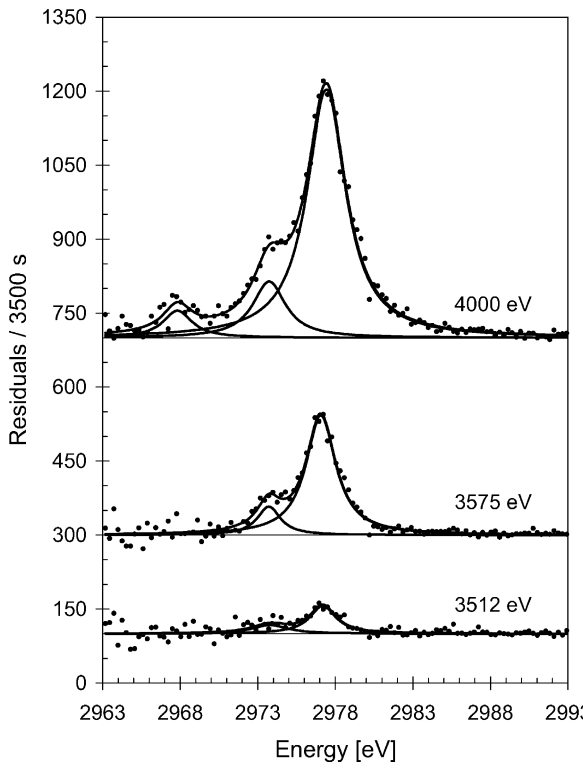

Fig. 1. The argon KL-$L_{2,3}$L satellite double electron excitation X-ray spectra at three different X-ray beam energies. The overall profiles of the X-ray satellite spectra corresponds to the sum of many components resulting from the coupling between K and L holes in the initial state and 2L holes in the final state. The lowest energy component appearing above the threshold for 1s–2s excitation, corresponds to the decay of 1s–2s double-vacancy states.

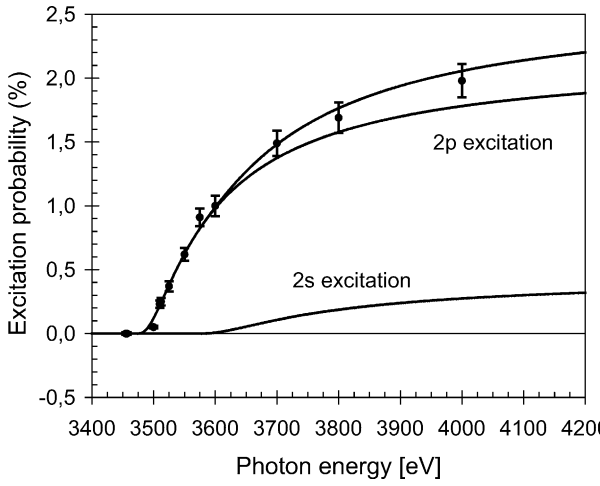

Fig. 2. Evolution of the Ar KL double excitation probability with the incident X-ray beam energy. The solid lines represent the fit to the Thomas model.

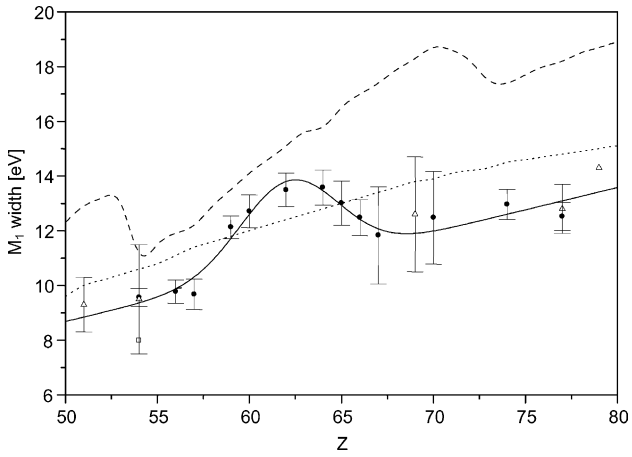

Fig. 3. M_1 atomic level width vs. atomic number Z. Black circles (●) correspond to the results of this work. The solid line represents a least-squares fit to the present results, the dotted line the recommended values of Campbell and Papp [13], the dashed line represents results of independent-particle model calculations by Perkins et al. [14]. Several experimental data from different sources are also presented, using the following symbols: (△) X-ray emission spectroscopy results from Refs. [15–18], (□) values provided with X-ray photoelectron spectroscopy taken from Ref. [19].

represented by the solid lines in Fig. 2. From the comparison, the onset energies (E_{thr}) for the 2s and 2p excitations could be determined as well as the high-energy limit of the shake probability (P_∞), and the radius r of the 2p orbital in ionic Ar. For 2p excitation $P_\infty = 2.19 \pm 0.04\%$ and $E_{\mathrm{thr}} = 3462 \pm 6\,\mathrm{eV}$, while for 2s excitation $P_\infty = 0.45 \pm 0.01\%$ and $E_{\mathrm{thr}} = 3544 \pm 6\,\mathrm{eV}$ and $r = 0.14 \pm 0.01\,\text{Å}$.

4. L_3 and M_1 atomic-level widths of elements $54 \leq Z \leq 77$

In view of a lack of modern XES data on M_1 level widths in the region $54 \leq Z \leq 77$, as pointed out recently by Campbell and Papp [13], our main objective was to establish a new set of experimental M_1 level widths for $_{54}$Xe, $_{56}$Ba, $_{57}$La, $_{59}$Pr, $_{60}$Nd, $_{62}$Sm, $_{64}$Gd, $_{65}$Tb, $_{66}$Dy, $_{67}$Ho, $_{70}$Yb, $_{74}$W and $_{77}$Ir. Spin-off results are reliable experimental data concerning the L_3 level widths and L_3–M_4, L_3–M_5 and L_3–M_1 X-ray transition energies for the thirteen investigated elements. Measurements of the L_3–M_5 and L_3–M_1 fluorescence X-ray lines of elements $54 \leq Z \leq 77$ were performed with the high-resolution von Hamos spectrometer installed at both ID21 and BM5 beamlines at the ESRF in order to cover the required photon excitation energy range. The energy calibration of the spectrometer and the instrumental resolution was performed by measuring the $K\alpha_1$ X-ray lines of several 3d metals with $20 \leq Z \leq 32$. The X-ray spectra were fitted employing Voigt profiles and keeping fixed the Gaussian instrumental broadening.

Since M radiative yields are small and in addition L_3N double vacancy states may be created through L_1L_3N and L_2L_3N CK transitions or N-shell shake processes following the L_3-subshell photoionization resulting in nonradiative broadening of L_3 X-ray lines, the use of an intense and tunable monoenergetic X-ray beam is crucial. Photons whose energy is bigger than the L_3 edge but smaller than the $L_{1,2}$ edges can circumvent the unresolved N-satellites originating from $L_{1,2}L_3N$ CK transitions. Similarly, N-shell shake processes can be suppressed by using energies below the threshold energy for double $L_3 + N$ excitation.

The L_3 level widths of the investigated elements were determined from the differences between the measured linewidths of L_3–M_5 transitions and the M_5 level widths quoted in [13].

The M_1 levels were determined from the observed widths of L_3–M_1 transitions, employing for the L_3 widths the values from the present work. A precision of 3–6% was achieved, except for Ho and Yb where the total errors were comprised between 13 and 15%. A significant improvement was thus obtained with respect to the precision of the recommended values of Campbell and Papp (14–18%). Outside the lanthanide region a shift of about −2 eV was, however, observed between the two studies. In addition, in the lanthanide region, the M_1 level width follows a resonance curve which is not reported in [13]. The Z-dependence of the M_1 widths is related to the value of the total spin of the open 4f subshell and the exchange interaction with the 3s hole. The M_1 level width versus atomic number Z is depicted in Fig. 3.

5. 3p–1s Mn RIXS spectra of manganese oxides

Recently, a RIXS study of manganese oxides was undertaken with the intention to extend it to manganese oxide compounds (manganites) that have attracted a lot of attention in the last years [1,20].

High-resolution measurements of RIXS spectra of metallic manganese and manganese oxides such as MnO, MnO_2,

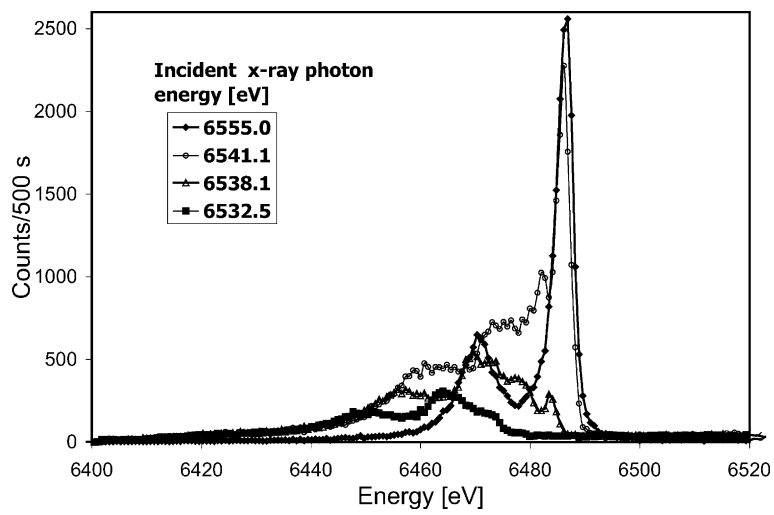

Fig. 4. MnO 3p–1s XES and the evolution of RIXS spectra with several incident X-ray photon energies across the Mn K-edge.

Mn_3O_4 and Mn_2O_3 using X-ray synchrotron radiation were performed. By tuning the incident photon energy across the K-edge (6.539 keV) of Mn different intermediate states can be probed. For illustration, the evolution of the MnO RIXS spectra with the incident energy, reflecting radiative transitions from specific intermediate states determined by the incident photon energy to final states, is depicted in Fig. 4. The variation in position, yield and profile of the Mn Kβ X-ray emission lines and the RIXS spectra depend on the oxidation and the spin states of the Mn sites as well as on d-electron correlation and inter-atomic hybridization. A comparison to theoretical predictions could bring further insight into intra-atomic multiplet coupling, electron correlation and inter-atomic hybridization. Since in transition metal compounds, the electron correlation strength is intermediate between semiconductors and rare-earths systems, these materials represent an interesting regime to study the interplay between the itinerant and local character of 3d electrons.

6. Concluding remarks

The main objective of the presented review of the X-ray emission studies performed with the von Hamos bent crystal Bragg X-ray spectrometer at an X-ray synchrotron radiation facility, was to illustrate its potential in XES and RIXS studies. The high-resolution in a wide energy range and versatility of the instrument in combination with X-ray synchrotron radiation represents a powerful tool in the metrology of X-ray transitions and in understanding electronic structure. Further projects are foreseen in the field of XES and RIXS.

Acknowledgements

This work was supported by the European Synchrotron Radiation Facility (ESRF) and the Swiss National Science Foundation.

References

[1] A. Kotani, S. Shin, Rev. Mod. Phys. 73 (2001) 203.
[2] J. Hoszowska, J.-Cl. Dousse, J. Kern, Ch. Rhême, Nucl. Instr. Methods A 376 (1996) 129.
[3] J.-Cl. Dousse, J. Hoszowska, Phys. Rev. A 56 (1997) 4517.
[4] J. Hoszowska, J.-Cl. Dousse, D. Castella, D. Corminboeuf, J. Kern, Y.-P. Maillard, P.-A. Raboud, J. Phys. B: At. Mol. Opt. Phys. 33 (2000) 3165.
[5] P.-A. Raboud, J.-Cl. Dousse, J. Hoszowska, I. Savoy, Phys. Rev. A 61 (2000) 012507.
[6] O. Mauron, J.-Cl. Dousse, Phys. Rev. A 66 (2002) 042713.
[7] P.-A. Raboud, M. Berset, J.-Cl. Dousse, Y.-P. Maillard, O. Mauron, J. Hoszowska, M. Polasik, J. Rzadkiewicz, Phys. Rev. A 65 (2002) 062503.
[8] O. Mauron, J.-Cl. Dousse, S. Baechler, M. Berset, Y.-P. Maillard, P.-A. Raboud, J. Hoszowska, Phys. Rev. A 67 (2003) 032506.
[9] R.D. Deslattes, R.E. La Villa, P.A. Cowan, A. Henins, Phys. Rev. A 27 (1983) 923.
[10] M. Deutsch, O. Gang, K. Hämäläinen, C.C. Kao, Phys. Rev. Lett. 76 (1996) 2424.
[11] C. Sternemann, A. Kaprolat, M.H. Krisch, W. Schülke, Phys. Rev. A 61 (2002) 020501.
[12] T.D. Thomas, Phys. Rev. Lett. 52 (1984) 417.
[13] J.L. Campbell, T. Papp, At. Data Nucl. Data Tables 77 (2001) 1.
[14] S.T. Perkins, D.E. Cullen, M.H. Chen, J.H. Hubbell, J. Rathkopf, J.H. Scofield, Tables and Graphs of Atomic Subshell Relaxation Data derived from the LLNL Evaluated Atomic Data Library, Lawrence Livermore National Laboratory Report UCRL-50400, vol. 30, 1991.
[15] M. Ohno, R.E. La Villa, Phys. Rev. A 45 (1992) 4713.
[16] T. Papp, J. Campbell, J.A. Maxwell, J.X. Wang, W.J. Teesdale, Phys. Rev. A 45 (1992) 1711.
[17] F.K. Richtmeyer, S.W. Barnes, E. Ramberg, Phys. Rev. 46 (1934) 843.
[18] M. Ohno, P. Putila-Mantyla, G. Graeefe, J. Phys. B: At. Mol. Phys. 17 (1984) 1747.
[19] S. Svensson, N. Martensson, E. Basilier, P.A. Malmqvist, U. Gelius, K. Siegbahn, Phys. Scripta 14 (1976) 141.
[20] T. Inami, T. Fukuda, J. Mizuki, S. Ishihara, H. Kondo, H. Nakao, T. Matsumura, K. Hirota, Y. Murakami, S. Maekawa, Y. Endoch, Phys. Rev. B 67 (2003) 045108.